

Photo isomerization of *cis*-cyclooctene to *trans*-cyclooctene: Integration of a micro-flow reactor and separation by specific adsorption

Elnaz Shahbazali¹  | Emilie M. F. Billaud² | Arash Sarhangi Fard³ | Jan Meuldijk¹ | Guy Bormans² | Timothy Noel¹ | Volker Hessel¹

¹Department of Chemical Engineering and Chemistry, Micro Flow Chemistry and Process Technology, Eindhoven University of Technology, Eindhoven, The Netherlands

²Laboratory for Radiopharmaceutical Research, Department of Pharmaceutical and Pharmacological Sciences, KU Leuven, Leuven, Belgium

³Materials Technology Institute, Eindhoven University of Technology, Eindhoven, The Netherlands

Correspondence

Timothy Noel and Volker Hessel, Department of Chemical Engineering and Chemistry, Micro Flow Chemistry and Process Technology, Eindhoven University of Technology, Eindhoven, The Netherlands.
Email: t.noel@tue.nl (T. N.) and volker.hessel@adelaide.edu.au (V. H.)

Funding information

European Research Council, Grant/Award Number: 267443

Abstract

Liquid-phase adsorption has hardly been established in micro-flow, although this constitutes an industrially vital method for product separation. A micro-flow UV-photo isomerization process converts *cis*-cyclooctene partly into *trans*-cyclooctene, leaving an isomeric mixture. *Trans*-cyclooctene adsorption and thus separation was achieved in a fixed-bed micro-flow reactor, packed with AgNO₃/SiO₂ powder, while the *cis*-isomer stays in the flow. The closed-loop recycling-flow has been presented as systemic approach to enrich the *trans*-cyclooctene from its *cis*-isomer. In-flow adsorption in recycling-mode has hardly been reported so that a full theoretical study has been conducted. This insight is used to evaluate three process design options to reach an optimum yield of *trans*-cyclooctene. These differ firstly in the variation of the individual residence times in the reactor and separator, the additional process option of refreshing the adsorption column under use, and the periodicity of the recycle flow.

KEYWORDS

flow chemistry, microreactor, isomerization, photochemistry, process integration

1 | INTRODUCTION

In cancer discovery research, radiolabeled monoclonal antibodies directed against tumor-associated antigens have been developed as promising vectors to visualize or to treat tumors, mostly owing to their high affinity and specificity.^{1,2} Since antibodies have a long biological half-life, it takes a long time (in the order of days) to clear the antibodies from plasma. The half-life of radionuclides that are used to radiolabel antibodies should be sufficiently long (>12 hr) to allow clearance of the radiolabeled antibody from plasma prior to acquire high signal-to-noise ratio tumor PET images. The use of long lived radionuclides (e.g., ⁶⁴Cu, ¹²⁴I, ⁸⁹Zr) will however result in prolonged

exposure to radiation and a high absorbed radiation dose. Fluorine-18 (F-18) is the most frequently used radionuclide for positron-emission tomography (PET)³⁻⁵ radioisotopes due to its favorable physical properties (e.g., half-life of 109.8 min).⁶

Application of short-lived F-18 for in vivo visualization of antibodies can be achieved by pretargeting approaches based on high yield in vivo click reaction using for example, ¹⁸F-labeled *trans*-cyclooctene (TCO) or tetrazine derivatives.⁷ This reaction strategy has been used for both in vitro and in vivo applications.^{5,8,9}

Trans-cyclooctene has a high reactivity due to the release of high strain energy upon the click reaction providing a well-defined chiral structure, which makes it interesting for stereocontrolled synthesis.

This is an open access article under the terms of the Creative Commons Attribution-NonCommercial License, which permits use, distribution and reproduction in any medium, provided the original work is properly cited and is not used for commercial purposes.

© 2020 The Authors. *AIChE Journal* published by Wiley Periodicals LLC on behalf of American Institute of Chemical Engineers.

Therefore, radiolabeled TCOs are good candidates for bio-orthogonal chemistry.¹⁰

There are many routes to synthesize a *trans*-cyclooctene. A common and elegant way is the photoisomerization of *cis* to *trans*-cyclooctene.¹¹ Yet, the photoisomerization is not irreversible and thus removal of the *trans*-isomer from the equilibrium *cis* and *trans* mixture is required to shift the equilibrium. Fox et al. have proposed an elegant procedure for the photochemical synthesis of TCO.¹² In this method, TCO was produced via photoisomerization of *cis*-cyclooctene by exposure to UV light (254 nm) in a batch vessel. The reaction mixture was continuously passed through a bed of silver nitrate impregnated on silica gel. Subsequently, the TCO is selectively retained by silver nitrate and the remaining *cis*-cyclooctene-containing solution is recycled to the photochemistry batch vessel. This is a very unique method yet the total yield was 66% and the total reaction time was relatively long, that is, 12 hr.

Recently, the sustainable production of active pharmaceuticals and excipients has received a lot of attention.¹³ Novel bioprocesses, continuous-flow processing, process integration, and intensification and green chemistry are the main assets of sustainable processes. Flow chemistry, especially micro-flow technology, is a high potential platform in terms of equipment size reduction, energy efficiency, and reduced solvent usage to achieve process intensification and thereby performing more sustainable processes in fine chemistry.^{14,15}

More specifically, for photochemical reactions, microreactors have several advantages compared to batch processes such as improved photon transport, energy efficiency, and better mixing.¹⁶⁻¹⁸ The constricted diameter of the microreactors (shorter photon diffusion pathway) allows better use of the irradiated light efficiently reducing the total exposure time, which leads to shorter reaction time and possibly reduced byproduct formation.^{19,20}

Beyond microfabricated channels, and microcapillaries, mini-scale packed-bed reactors allow to form micro-flow in their void spaces. Indeed, enhanced reaction rates, higher conversions, and selectivities were found as well and can be attributed to the reduced mass-transfer limitations.^{21,22} This, in combination with the high surface-to-volume ratio, makes the packed-bed reactor suited for performing biphasic reactions in multiple-repeated reentrance-flow mode or for heterogeneous catalytic reactions.²³ Adsorption (and desorption) is an essential step in heterogeneous catalysis. Hernández Carucci et al. proposed a model based on the competitive adsorption of ethylene and molecular oxygen over a silver surface of microchannels at 260°C as part of a precise kinetic model for the ethylene oxide formation.²⁴

Accordingly, it stands to reason that sole adsorption processes (without catalysis) might be intensified in micro-flow. Microspheres have been reported and termed as adsorption “microreactors” and indeed use the same transfer intensification by size reduction.²⁵ Rutin-Cr(III) loaded alginate microspheres were designed to reduce Cr(VI) to Cr(III) through adsorption and recover it. Also, there is an ongoing efforts in the development of inflow separation by using solid adsorbent and scavengers in organic synthesis, especially for isolation of drug substances.²⁶⁻²⁹ Yet, true micro(channel)reactors and micro-flow packed bed reactors have been hardly applied for adsorption so far.

Recently, we reported on the combination of a nucleophilic substitution to the thermal-Claisen rearrangement and also to photo-Claisen rearrangement in micro-flow.^{30,31} The motivation was to integrate two processes and to address the resulted challenging issues toward orthogonality. Also, here, we would like to design and integrate two processes, photoreaction and adsorption, yet with more in depth theoretical study for each process.

Therefore, the aim of this study is to develop a photo micro-flow process for the photochemical isomerization of *cis*-cyclooctene to TCO and its subsequent in-flow separation to isolate isomerically pure TCO derivatives. Such a compact integration of small devices fed with minute volumes provides opportunities for synergism between reaction and separation, which is a means of process intensification and was termed process-design intensification³² as one arms of novel process windows.³²⁻³⁴

More specifically, we focus in this work on the experimental procedures (batch as well as flow) for the photoisomerization, and the design and operation of the adsorption column. Furthermore, the theoretical concepts behind these operations are explained and relevant models for both sections are developed. Finally, the results of the experiments and theoretical modeling are presented and discussed.

2 | EXPERIMENTAL SECTION

2.1 | Chemicals

Cis-cyclooctene, methyl benzoate, *n*-dodecane, AgNO₃/Silica (10% loading, +230 mesh size), ammonium hydroxide (28% NH₃ in H₂O), 1,3,5 trimethoxy benzene, *n*-hexane, diethyl ether, and dichloromethane were purchased from Sigma-Aldrich chemical company and used as received. The solvent purity were all according to HPLC grade (>95%). Ultrapure water (HPLC grade, 18.2 MΩ at 25°C) was used.

2.2 | *Trans*-cyclooctene preparation

It is referred to Supporting Information.

2.3 | Batch operation for determination of the adsorption isotherm

The batch adsorption experiment was performed in 25 ml glass Erlenmeyer flask at a fixed temperature, 23°C. The first experiment was done by concentrating the pure TCO in *n*-hexane to a volume of approximately 5 ml. Then 0.192 mmol of 1,3,5 trimethoxybenzene (internal standard for ¹H-NMR) was added. Based on the ¹H-NMR result, the amount of TCO was calculated. Then, a fixed amount (0.2 g) of AgNO₃/silica was added to the solution. Subsequently, the Erlenmeyer was shaken at 100 rpm in a temperature controlled shaker, for a period of 4 hr. Next, the mixture was kept in stagnant

mode to let the particles sediment. From the solution a sample (0.2 ml) was taken for $^1\text{H-NMR}$ analysis. The result is one point in the TCO adsorption isotherm. Afterward, 3 ml of *n*-hexane was added to the solution and was shaken again at the same condition as previous for a period of 4 hr and consequently another sample was taken for $^1\text{H-NMR}$ analysis. This procedure was repeated for several times and every time a certain amount of solvent was added and after shaking a sample was taken for $^1\text{H-NMR}$ analysis.

The amount of solute (B) adsorbed per gram dry of adsorbent at equilibrium, q_B (g_B/g), was calculated according to Equation (1).

$$q_B = \frac{V}{W}(C_{B_0} - C_{B_e}) \quad (1)$$

Where, C_{B_0} (g/dm³) and C_{B_e} (g/dm³) are respectively the initial and equilibrium concentrations of the solute (B) in the liquid phase, V (dm³) is the solution volume, and W (g) is the weight of the dry adsorbent.

2.4 | Continuous flow setup

The experimental setup used for micro-flow based photoisomerization and in-flow separation process is presented in Section S1. The solution is pumped from the inlet solution vessel using an HPLC pump (Knauer Azura P4.1S). The outlet stream from the pump is fed to FEP (fluorinated ethylenepropylene copolymer, IDEX 1548L) capillary tubular reactor (ID 0.02", OD 1/16", length 5 m) which is wound around a cylindrical UV light source placed inside a closed oven. Irradiation is carried out using a low-pressure amalgam lamp (TS23-212; Dinies Technologies GmbH). The outlet then flows to the packed bed. The packed bed (stainless steel, ID 4.5 mm, L 25 mm) is packed with 200–220 mg of AgNO₃ impregnated silica gel (as packing or adsorbent) with a mesh size of 230+ (Sigma-Aldrich). The AgNO₃/silica particles are mixed with 1 mm borosilicate glass beads in a mass ratio 1.66:1 and then introduced to the packed bed with a funnel. The inert glass beads are applied to prevent particle agglomeration which results in channeling of the flow inside the packed bed (for more information on micropacked beds and the assembling process, we refer to References 35-37). The inlet and outlet of the packed bed have attached separately two frits with a pore size of 10 μm to keep the packing material inside the reactor. The outlet of the packed bed is recycled to the inlet solution vessel through a 0.2 m long FEP capillary tube. Samples are collected exactly before the recycle stream enters the inlet solution vessel. The inlet solution vessel is stirred with a magnetic stirrer bar to ensure a uniform concentration in the vessel. In a general micro-flow based photoisomerization and an in-flow separation experiment, *cis*-cyclooctene (0.06 g, 0.55 mmol), methyl benzoate as a singlet sensitizer (0.136 g, 1 mmol), and *n*-dodecane as the internal standard for GC analysis (0.017 g, 0.1 mmol) are dissolved in 25 ml *n*-hexane (with 1% diethyl ether) as solvent and mixed in the same vessel (volumetric flask of 50 ml) and from this vessel the solution is pumped to the flow setup.

2.4.1 | Photo-microreactor kinetics study experiment

In order to perform a kinetic study of the photoisomerization, *cis*-cyclooctene (0.0234 g, 0.2 mmol), methyl benzoate (0.054 g, 0.4 mmol) and *n*-dodecane (0.014 g, 0.082 mmol) are dissolved in 10 ml *n*-hexane and mixed well. This solution is pumped in to the photo-microreactor (FEP tubing, 2 m) without passing the packed bed. The reaction mixture is not recycled. The flow rate is varied between 0.02 and 1.0 ml/min, corresponding to mean residence times of 10–0.20 min. The samples are collected for GC analyses at the outlet of photo-microreactor for each flow rate.

2.4.2 | Breakthrough curve prediction experiment

The experiment was done by concentrating pure TCO in *n*-hexane to a volume of 12.75 ml. Then 0.02141 g 1,3,5 trimethoxybenzene (internal standard for $^1\text{H-NMR}$) was added. Based on the $^1\text{H-NMR}$ result, the amount of TCO was calculated which was equal to 0.04 g (0.028 mol/dm³). Then the solution was diluted to 20 ml ([TCO], 0.018 mol/dm³). The packed bed (stainless steel, ID 4.5 mm, L 25 mm) was packed with 0.2 g AgNO₃/silica and 0.12 g glass beads (1 mm), similarly to the previous section. The inlet solution is pumped through the packed bed at the flow rate of 1 ml/min. The outlet of the packed bed was connected to a FEP tube, from which samples were collected for analyses. All packed bed space times have been determined assuming a bed porosity of 0.5.

2.5 | Characterization

It is referred to Supporting Information.

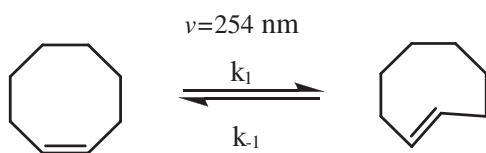
3 | THEORETICAL STUDY

3.1 | Photoreactor

It is known from the literature^{11,38,39} that the photoisomerization of *cis* to *trans*-cyclooctene is an equilibrium reaction. However, we could not find an in depth kinetic study about this photoisomerization. To investigate the kinetics of the equilibrium reactions, the conversion time histories have been monitored. The results reveal the existence of equilibrium between the *cis* and *trans*-isomers.

3.2 | Kinetics of the photoisomerization

When it is assumed that intrinsic kinetics is obeyed and that the photoreaction follows the first order kinetics, the



SCHEME 1 Photo isomerization of *trans* from *cis*-cyclooctene

photoisomerization of *cis*-cyclooctene to *trans*-cyclooctene is represented in Scheme 1:

For a first order reversible reaction,⁴⁰ in the ideally mixed batch reactor, the concentration of the *cis*-cyclooctene C_{cis} as a function of time obeys Equation (2):

$$\frac{C_{cis}(\tau)}{C_{cis}(0)} = \left[\frac{1}{k_1 + k_{-1}} \left(k_1 e^{-\tau(k_1 + k_{-1})} + k_{-1} \right) \right] \quad (2)$$

$C_{cis}(0)$ represents the concentration of *cis* at the start of reaction. See Supporting Information S2 for the derivation.

3.3 | Adsorption isotherm

An experimental adsorption isotherm correlates the adsorbed amount of the adsorbate (*trans*-cyclooctene) onto the adsorbent (AgNO_3) with the concentration of the adsorbate in solution at equilibrium at a fixed temperature.

3.4 | Langmuir isotherm

The Langmuir isotherm is one of the adsorption models that describe physisorption of neutral molecules onto adsorption sites.^{41,42} Based on the Langmuir model assumption, adsorption takes place on homogeneously distributed adsorbent sites by monolayer adsorption.

The nonlinearized Langmuir equation is expressed as:

$$q_{B_e} = \frac{b q_{\max} C_{B_e}}{1 + b C_{B_e}} \quad (3)$$

where q_{B_e} (mg/g) is the amount of TCO adsorbed by AgNO_3 at equilibrium, q_{\max} (mg/g) represents the maximum adsorption capacity, C_{B_e} (g/dm³) is the equilibrium concentration of the adsorbate in solution, and b (dm³/mg) is a constant that amongst others is related to the heat of adsorption.

Moreover, Equation (3) can be expressed as Equation (4).

$$\frac{C_{B_e}}{q_{B_e}} = \frac{C_{B_e}}{q_{\max}} + \frac{1}{q_{\max} b} \quad (4)$$

Plotting $\frac{C_{B_e}}{q_{B_e}}$ against C_{B_e} , allows the calculation of the parameters, b and q_{\max} .

3.5 | Packed bed modeling

In order to predict the dynamic behavior of the adsorption column, a mass balance over the liquid phase of an infinitesimal sized slice of the packed bed leads with perfect radial mixing and negligible pressure drop to Equation (5), see References 43-45.

$$D_{ax} \frac{\partial^2 C_i}{\partial z^2} - v \frac{\partial C_i}{\partial z} - \frac{1 - \epsilon_b}{\epsilon_b} N_i = \frac{\partial C_i}{\partial t} \quad (5)$$

In Equation (5), C_i , D_{ax} , v , ϵ_b , and N_i are the concentration of TCO in the liquid phase, the axial dispersion coefficient, the interstitial liquid velocity, the bed porosity, and the mass transfer rate into the particle per unit volume of the particle phase, respectively. The first and second term in Equation (5) stand for the dispersive transport and the convective transport in the column, respectively. The third term represents the mass transfer between liquid phase and adsorbent. The last term is related to accumulation of the adsorbate. This model is based on the following assumptions: isothermal adsorption and spherical adsorbent particles packed uniformly in the bed.

As it was stated, N_i is the mass transfer rate between solid and fluid phase and can be represented as⁴³⁻⁴⁵:

$$N_i = \rho_p \frac{\partial q_i}{\partial t} \quad (6)$$

$q_i \left[\frac{\text{mol}}{\text{kg}_s} \right]$ is the concentration of TCO on the adsorbent surface and $\rho_p \left[\frac{\text{kg}_s}{\text{dm}^3} \right]$ is the adsorbent particle density. In order to define $\frac{\partial q_i}{\partial t}$ mathematically, it is important to know whether the mass transfer resistance or the intrinsic adsorption kinetics dominates the adsorption rate.

3.6 | Mass transfer resistance and intrinsic adsorption rate

A useful approach to investigate and to compare the mass transfer resistance with the kinetic resistance is by comparing $\frac{1}{k_c a}$ with $\frac{1}{k_{ads}}$, i.e., the time constant for mass transfer and adsorption, respectively. Since the diameter of adsorbent particle is small, 60 μm , and the AgNO_3 layer thickness is much smaller than the silica particle diameter, the internal mass transport through the pores of the adsorbent has been neglected (for more information see Supporting Information S2). Therefore, the mass transfer resistance calculation is only based on the external mass transfer from the bulk fluid to the adsorbent surface.

Details for a "theoretical" estimation of the mass transfer coefficient from the bulk liquid to the outer surface of the particles in the packed bed (k_c) and the experimental determination of k_{ads} have been given in Supporting Information.

3.7 | Breakthrough curve prediction

The common available models in reported literature for breakthrough curve prediction are divided into two main categories based on the

existence of a mass transfer resistance between the adsorbent particles and fluid phase or local adsorption assumption between adsorbent particle and bulk phase, that is, by using intrinsic adsorption kinetics.⁴⁶

3.8 | Local adsorption model-local equilibrium theory

Local adsorption theory is divided into two sets of models depending on the rate of adsorption- local equilibrium theory and local kinetic theory.^{46,47}

Local equilibrium theory is based on the existence of equilibrium between adsorbate and fluid concentration, and how fast the equilibrium is reached in each stage in the packed bed column. Thus $\frac{\partial q_i}{\partial t}$ is defined by using the Langmuir isotherm as follows:

$$\frac{\partial q_i}{\partial t} = \frac{\partial q_i}{\partial C_i} \times \frac{\partial C_i}{\partial t} \quad (7)$$

and

$$\frac{\partial q_i}{\partial C_i} = \frac{q_{\max} b}{(1 + bC_i)^2} \quad (8)$$

where q_{\max} and b are from Langmuir isotherm model, see Equation (3).

The local kinetic theory is based on a non-equilibrium adsorption reaction. It is expressed based on the rate of adsorption and desorption of the adsorbate on the surface of adsorbent particles.

In this work an equilibrium surface reaction is governing, so the only model that has been applied is the local equilibrium theory. For the local kinetic theory, see the related literature.^{46,47}

Therefore, Equation (5) becomes

$$D_{ax} \frac{\partial^2 C_i}{\partial z^2} - v \frac{\partial C_i}{\partial z} = \left[1 + \rho_p \frac{(1 - \varepsilon_b)}{\varepsilon_b} \times \frac{q_{\max} b}{(1 + bC_i)^2} \right] \frac{\partial C_i}{\partial t} \quad (9)$$

For the model calculations the partial differential Equation (9) has to be solved. Equation (9) is discretized using finite differences and solved using MATLAB[®] with implicit PDEPE solvers.

The initial condition is a packed bed filled with solvent. Then, at the inlet of the column a step change is applied. The applied boundary conditions are of Danckwert's type conditions⁴⁸ and used at the inlet ($z = 0$) and at the outlet ($z = L$) of the column (Equation 10).

$$\frac{\partial C_i}{\partial z} \Big|_{z=0} = \frac{v}{D_{ax}} (C_i - C_{i,feed}); \frac{\partial C_i}{\partial z} \Big|_{z=L} = 0 \quad (10)$$

The initial conditions are given by Equation (11)

$$C_i(z, t = 0) = 0 \quad (11)$$

3.9 | Modeling the combination of the photo-microreactor and the adsorption column

In this section it is aimed to predict the *cis*-cyclooctene conversion when there is a continuous closed system of the photo-microreactor with an integrated adsorption column and recycling the unreacted *cis*-isomer to the reactor feed solution (Figure 1). In order to mathematically model the system, two control volumes are selected: the photo-microreactor and the packed bed (1), and the stirred vessel with solution to be fed to the photoreactor (2).

The rate of photoisomerization of the *cis*-isomer into the *trans*-isomer has been given in the previous Section 3.1. It is assumed that the amount of the *cis*-isomer adsorbed in the packed bed is negligible. Therefore, for the first control volume and a single pass of the flow, if $C_t = \frac{n_{cis}}{V}$, where n_{cis} denotes the molar amount of the *cis*-isomer in the inlet vessel and V the volume of the photo-microreactor, the rate equation becomes (only if the outlet concentration of the *trans*-isomer from the packed bed is zero):

$$-\frac{dC_{cis}}{dt} = (k_1 + k_{-1}) \times C_{cis} - k_{-1} \times \frac{n_{cis}}{V} \quad (12)$$

The second control volume has been modeled by a mass balance of *cis* cyclooctene, see Equation (13). Note that the inlet vessel is ideally mixed.

$$\frac{dn_{cis}}{dt} + \frac{Q}{V} n_{cis} = Q \times C_{cis,iv} \quad (13)$$

where Q and $C_{cis,iv}$ stand, respectively for the total volumetric flow rate and the *cis* concentration at the inlet of the vessel. Equation (13) expresses the change in the amount of *cis*-isomer with respect to time. The concentration of *cis*-isomer at the outlet of the first control volume, (i.e., the outlet of the packed bed for *trans*-isomer adsorption)

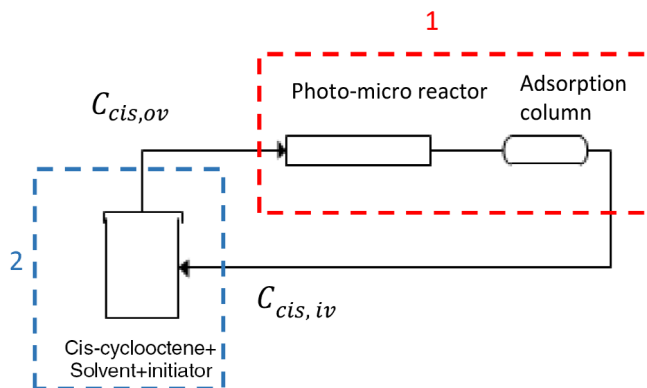


FIGURE 1 Schematic overview of the complete photo-microreactor and the adsorption system control volumes; (1): photo-microreactor and packed bed, (2): inlet vessel with reactor feed solution [Color figure can be viewed at wileyonlinelibrary.com]

is equal to the concentration of the *cis*-isomer at the inlet of control volume 2, (i.e., the vessel with the reactor feed solution) $C_{cis,iv} = C_{cis}$.

Equations (12) and (13) are solved simultaneously by using MATLAB[®] whereby the final concentration of *cis*-isomer or the final conversion of the *cis*-isomer with respect to time is obtained. The initial values for numerically solving Equation (12) and (13) are $C_{cis} = C_0$ and $n_{cis} = \frac{C_0}{V}$, where C_0 is the initial concentration of the *cis*-isomer in the reactor feed vessel.

4 | RESULTS AND DISCUSSION

4.1 | Kinetic study of photoisomerization

The photoisomerization of *cis*-cyclooctene into *trans*-cyclooctene has been investigated in detail in photo-microreactor. In order to determine the optimal reaction condition, the photoisomerization was performed at various residence times (for more details see Section 2). The results are presented in Figure 2. Figure 3 shows that conversion is limited by equilibrium to approximately 28%.

4.2 | k_1 and k_{-1} determination

The experimental data points in Figure 2 have been fitted to Equation 2. A regression analysis is carried out in MATLAB[®] (see Figure 2). k_1 and k_{-1} at 23°C are calculated to be 0.45 and 1.23 (1/min), respectively. For 23°C the equilibrium constant is $K = \left(\frac{C_{trans}}{C_{cis}}\right)_{eq} = \frac{k_1}{k_{-1}} = 0.36$.

4.3 | Adsorption isotherm

As stated before, the experimental adsorption isotherms represent the balance between adsorbent and adsorbate at equilibrium conditions. Figure 3 shows the adsorption isotherm for *trans*-cyclooctene on AgNO₃/silica at 23°C. Figure 3b clearly demonstrates that the

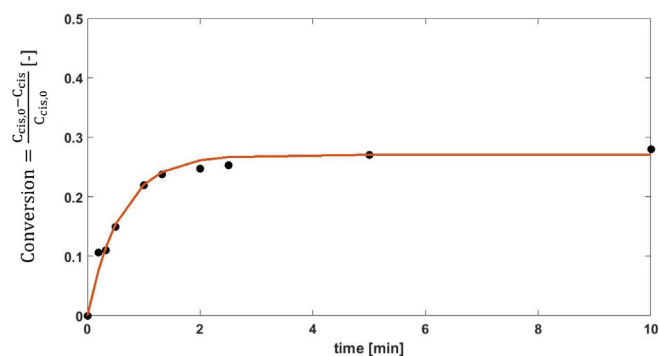


FIGURE 2 Results of regression analysis for calculating k_1 and k_{-1} . $X_{eq} = 0.28$ at 23°C, (•): experimental points; calculated line with Equation (2) and $k_1 = 0.45$ (1/min) and $k_{-1} = 1.23$ (1/min) [Color figure can be viewed at wileyonlinelibrary.com]

linear form of the Langmuir isotherm (Equation 4) is obeyed. The highest adsorption capacity was recorded at 43.089 mg/g at an initial concentration of 5.85 g/dm³.

Accordingly, the Langmuir model parameters, b and $q_{B,max}$, have been calculated 0.85 (dm³/g_{trans}) and 57.1×10^{-3} (g_{trans}/g_{AgNO3}), respectively.

4.4 | Adsorption kinetics

Adsorption kinetics of TCO on to AgNO₃/silica was studied by performing an experiment in batch, in which a known amount of AgNO₃/silica, (0.175 g) was suspended in the solution of TCO, $C_0 = 8.06$ g/dm³ in *n*-hexane. The time history of the liquid concentration of TCO was recorded, see Figure 4. In order to prevent any external mass transfer limitation, the suspension was stirred intensively. The experimental data were analyzed using (pseudo-)first-order and (pseudo-)second-order kinetics,⁴⁹⁻⁵³ see Equations (14) and (16), respectively:

$$\frac{dq_t}{dt} = k(q_{max} - q_t)^n \quad (14)$$

$n = 1$ for (pseudo-)first-order and $n = 2$ for (pseudo-)second-order

$$\ln\left(\frac{q_{B_e} - q_{B_t}}{q_{B_e}}\right) = -k't \quad (15)$$

$$\frac{1}{q_{B_t}} = \frac{1}{k''q_{B_e}^2} + \frac{1}{q_{B_e}} \quad (16)$$

Where k' (min⁻¹) and k'' (g mg⁻¹/min) are the rate constants for the (pseudo-) first and second-order kinetic models, respectively q_{B_e} and q_{B_t} are the amounts of the *trans*-isomer adsorbed per gram AgNO₃ at equilibrium and at time t , respectively. The constants can be calculated from the intercepts and slopes of the linear plots of $\ln(q_{B_e} - q_{B_t})$ versus t and t/q_{B_t} versus t , respectively (Figure 4).

Figure 4a shows that adsorption of *trans*-cyclooctene proceeds rapidly during the first 30s and becomes almost constant after 1 min. The adsorption rate constants and linear regression values are collected in Table 1. The results in Figure 4 and Table 1 reveal that adsorption obeys a (pseudo-)second order rate law. Also the experimentally observed value of q_{B_e} is equal to 44.3×10^{-3} g_{trans}/g_{AgNO3} and it can be easily observed that it is very close to q_{B_e} calculated from pseudo-second order kinetic model This fact suggests that the adsorption rate of *trans*-cyclooctene is dependent on the adsorption site availability on AgNO₃ rather than the *trans*-cyclooctene concentration in solution.^{54,55} Initially, there are many adsorption sites are available, however with the prolonging time the sites have been occupied, hence, limited free sites for molecule to be adsorbed on.^{54,56}

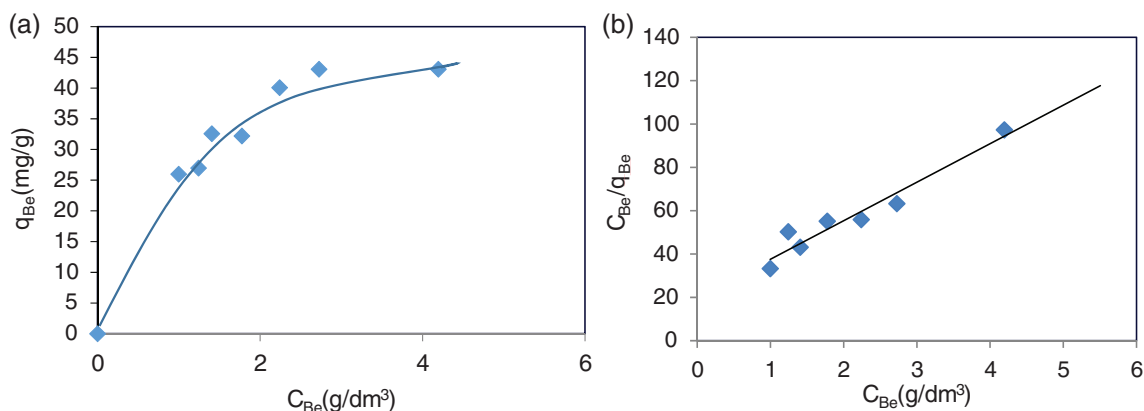


FIGURE 3 Adsorption isotherm of *trans*-cyclooctene on the $\text{AgNO}_3/\text{SiO}_2$ at 23°C , $W_{\text{AgNO}_3} = 0.175 \text{ g}$, $\frac{C_{\text{Be}}}{q_{\text{Be}}} = 17.515C_{\text{Be}} + 20.529$, $R^2 = 0.965$; (a) nonlinearized form and (b) linearized form (Equation 4) [Color figure can be viewed at wileyonlinelibrary.com]

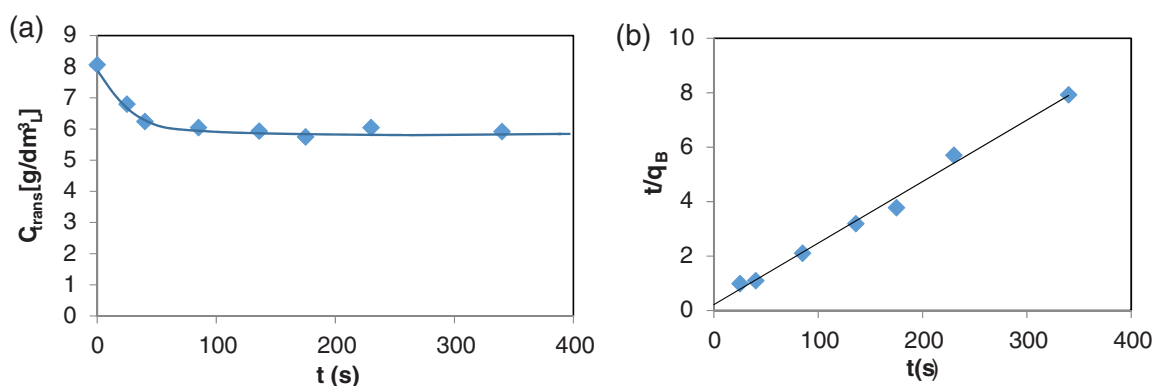


FIGURE 4 (a) Liquid phase concentration of *trans*-cyclooctene in a stirred vessel with a suspension of $\text{AgNO}_3/\text{SiO}_2$ in *n*-hexane (1% diethyl ether) $W_{\text{AgNO}_3/\text{SiO}_2} = 0.175 \text{ g}$, $C_0 = 8.06 \text{ g/dm}^3$ at 23°C , (b) (pseudo-)second-order kinetics for adsorption of *trans*-cyclooctene onto $\text{AgNO}_3/\text{SiO}_2$ [Color figure can be viewed at wileyonlinelibrary.com]

TABLE 1 pseudo-second-order rate constant for adsorption of TCO onto AgNO_3 at 23°C

Models	Model parameters	R^2
(pseudo-)first-order	$q_{\text{Be}} = 15.87 \text{ mg/g}$ $k' = 8.8 \times 10^{-3} \text{ min}^{-1}$.69
(pseudo-)second-order	$q_{\text{Be}} = 44.25 \text{ mg/g}$ $k'' = 0.51 \times 10^{-3} \text{ g}_{\text{AgNO}_3} \text{ mg}^{-1} \text{ trans min}^{-1}$.9924

4.5 | Packed bed

4.5.1 | Breakthrough model validation

In order to validate the model (see Equations 9–13), the obtained results from the adsorption breakthrough curve model are compared with the experimental results, see Figure 5. The calculated breakthrough curve agrees reasonably well with the experimentally observed curve. The proposed breakthrough curve model is able to predict the saturation time, t_s , of the adsorption column. t_s is the time at which $\frac{C_{\text{trans}}}{C_{\text{trans}0}} = 0.05$.

4.5.2 | Process design for integration of a photo-microreactor and adsorption for the isomerization of *cis*-cyclooctene in to *trans*-cyclooctene

After optimizing each sub process, that is, photoisomerization and adsorption, in this section, the process configuration for photoisomerization of *cis* into *trans*-cyclooctene is presented for three different cases. These three cases were experimentally tested. The model for the adsorption column that was presented earlier in this paper, can be used to estimate saturation time and the operational parameters such as the temperature for the adsorption of *trans*-cyclooctene. Later in the text the validity of the model as described in Section 3.3 is confirmed with the experimental results.

4.5.3 | Solvent selection

The selection of a proper solvent is crucial in any (photo)chemical reaction. Here, this is even more significant as the solvent should play a role in different process steps. First, it should be able to solubilize

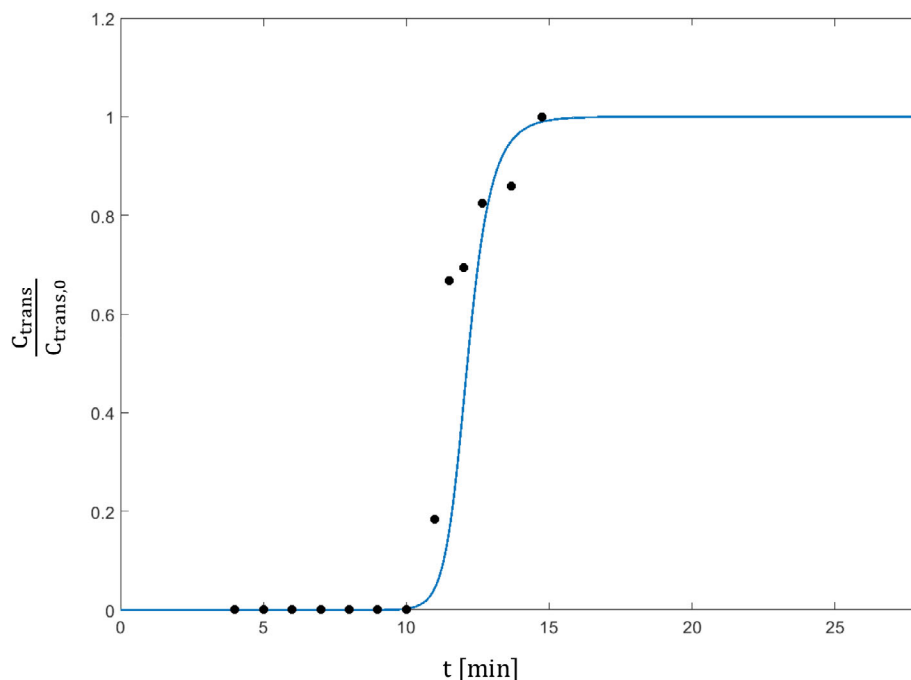


FIGURE 5 Calculated and experimental breakthrough curve at 23°C, $W_{AgNO_3} = 0.2$ g, volumetric flow rate = 1 mL/min, $C_{trans0} = 1.99$ g/dm³ [Color figure can be viewed at wileyonlinelibrary.com]

the cyclooctene (both *cis*- and *trans*-) and the sensitizer. Also, the solvent has to be transparent at the required wavelength, 245 nm. On the other hand, it should not dissolve the packing powders ($AgNO_3$ /silica). If $AgNO_3$ dissolves, the *trans*-complex will not be collected in packed bed and there is no separation of the *trans*-isomer from the *cis*-isomer. This means that there is no equilibrium shift in the direction of the *trans*-isomer. Considering the features mentioned, *n*-hexane or cyclohexane seems to be proper choices. Cyclohexane has a higher boiling point than *n*-hexane. Since to desorb *trans*-cyclooctene from $AgNO_3/SiO_2$ there is an elution step needed which is not included in this process design. Therefore, as the solvent of this process, *n*-hexane is preferred. Also, in order to increase the solubility of *cis* and *trans*-cyclooctene 1% of diethyl ether is added. It is worth mentioning that diethyl ether dissolves $AgNO_3$, so it is recommended not to increase the ratio of diethyl ether to *n*-hexane to more than 5:95 (volume ratio).

4.5.4 | Process configurations

Case (a). This case concerns the basic continuous flow setup in which a photo-microreactor of 5 m length and an adsorption column of 5 cm length packed with $AgNO_3/SiO_2$ powders are used (Figure 6a). The flow rate is set to 0.2 ml/min. As reported earlier in Section 2.4, in all cases the outlet flow from the packed bed is recycled to the vessel with the reactor feed solution.

Case (b). Since, our system is a closed-loop recycle flow system, it is important that as soon as photoreaction takes place the molecules are transferred to the separation unit and from there quickly recycled to the feed vessel. Therefore, the key in this design (Case b) is to

reduce the residence time of the flowing fluid in the connecting tubes and parts between the feed vessel, the photo-microreactor(s), and the packed bed.

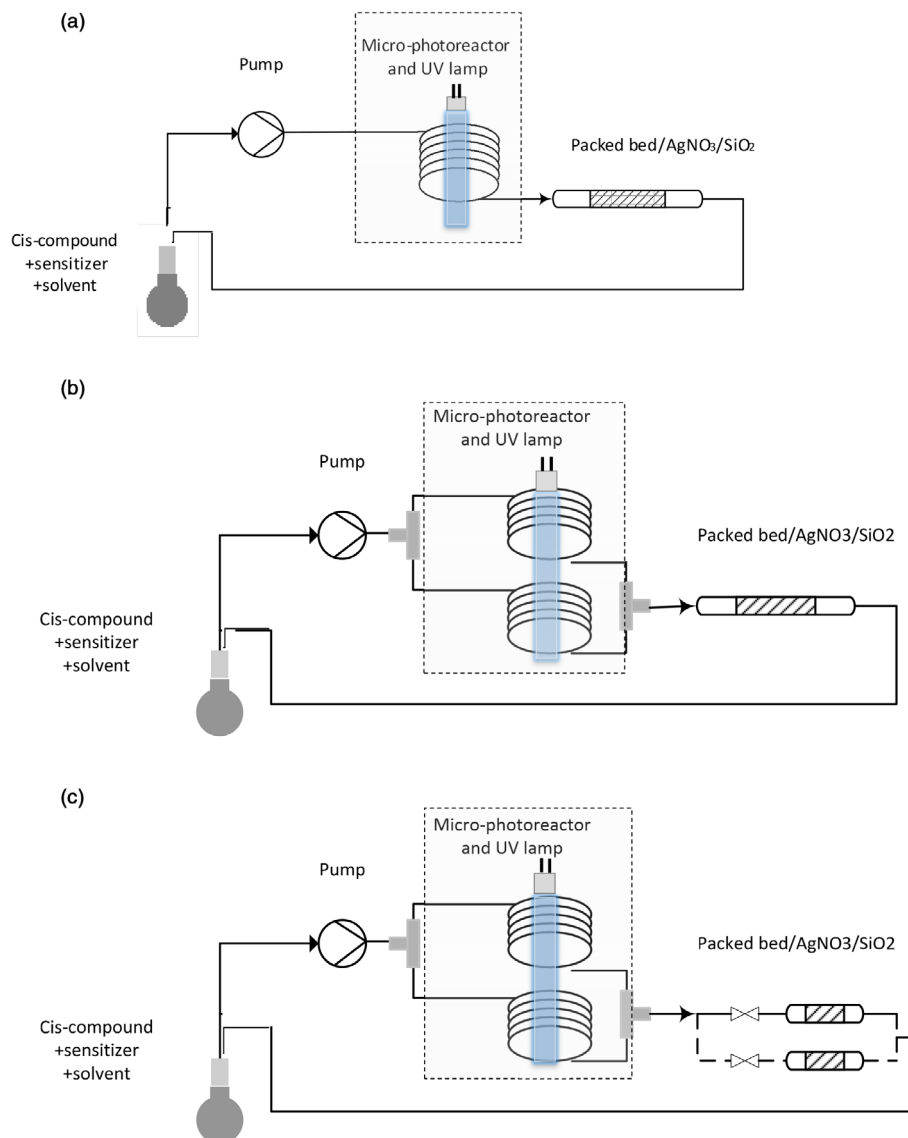
In this case, we applied the concept of symmetrical flow splitting by using a T-micromixer placed in reverse mode to act as flow splitter in a bifurcate fashion the feed flow rate is directed toward two photo-microreactors of 5 m length which are wound around one UV light and placed in parallel (Figure 6b). With this design, it is possible to double the main flowrate while keeping the residence time in the photo-microreactor the same as in Case (a).

Therefore, the total flow rate is raised to 0.4 ml/min, which speeds up the flow in connecting parts, and by symmetrical flow splitting, the flow rate is kept 0.2 ml/min in each photo-microreactor.

Case (c). This case is similar to the Case b. Again, two parallel photo-microreactors are used. But, the main difference is that in this configuration more than one packed bed, each with a length of 2.5 cm, are installed in parallel, see Figure 6c. This adds the function of refreshing the adsorption column under use, by switching between two columns set in parallel—one for the closed-loop flow and the other in a wait position, being re-activated. Such an integrated flow configuration for purification following micro-flow reaction was already proposed by us in a recent paper, using a fixed-bed column packed with Amberlyst resin for an ion-exchange based purification of the product mixture.³⁰

In the operational mode, the parallel packed beds are connected to the photoreactor by a switching valve. While one packed bed is in use to adsorb the *trans*-isomer, the other is in the waiting mode. As soon as the first column reaches saturation, the flow is switched to pass through a fresh packed bed. Based on the amount of the inlet *cis*-cyclooctene, in this case, three parallel packed beds are used. Also, the flow rate is increased to 0.66 ml/min.

FIGURE 6 Three different process configuration for photoisomerization of *cis* to *trans*-cyclooctene. Case (a), Case (b), Case (c) [Color figure can be viewed at wileyonlinelibrary.com]



4.5.5 | Validation of the model in the combination of micro photoreactor and adsorption column

The results in Figure 7 demonstrate that the conversion of *cis*-cyclooctene as a function of the process time obtained from solving the model discussed in Section 3.3. This model has been solved and sketched for different total flow rates and compared with each experimental case. Here, time is the total operational time.

In Case (a) after 400 min almost 70% conversion is achieved. This time is the total required time of operation since this is a closed-loop system operating in a recycling mode. In the Case (b), as stated earlier the total flow rate is doubled to 0.4 ml/min, while the residence time in each photoreactor is the same as in Case (a). Figure 7b shows that there is a small deviation between the results of the model calculations and the experimental results. Besides, upon increasing the total operational time, the deviation increases and at some point the experimental results tend to reach a plateau earlier than with the predicted model. Since the total flow rate is doubled, the flow rate inside the

packed bed is also doubled. Therefore, the packed bed reaches saturation earlier in Case (b) than in Case (a). With prolonging time, the packed bed becomes saturated with TCO and TCO molecules are not adsorbed anymore and recycled in the system which also affects the photoreaction process to reach equilibrium faster. As a result, the total conversion of *cis*-cyclooctene is not improved anymore and therefore the experimental points tend to reach a plateau and deviate from the model.

In Case (c), there is less deviation between the experimental points and the results of the model calculations (Figure 7c). The first switching toward a fresh packed bed was at 75 min operational time and the second switch was at 180 min. As indicated in Figure 7c, after 50 min the packed bed tends to reach saturation. Therefore there is a plateau before the fresh packed bed was in use (75 min) which explains the small deviation between the experimental results and the results of model calculations. Also, it is important to note that this is a closed system and the concentration of the *cis*-isomer is getting less with respect to the operational time. Therefore, the first packed bed

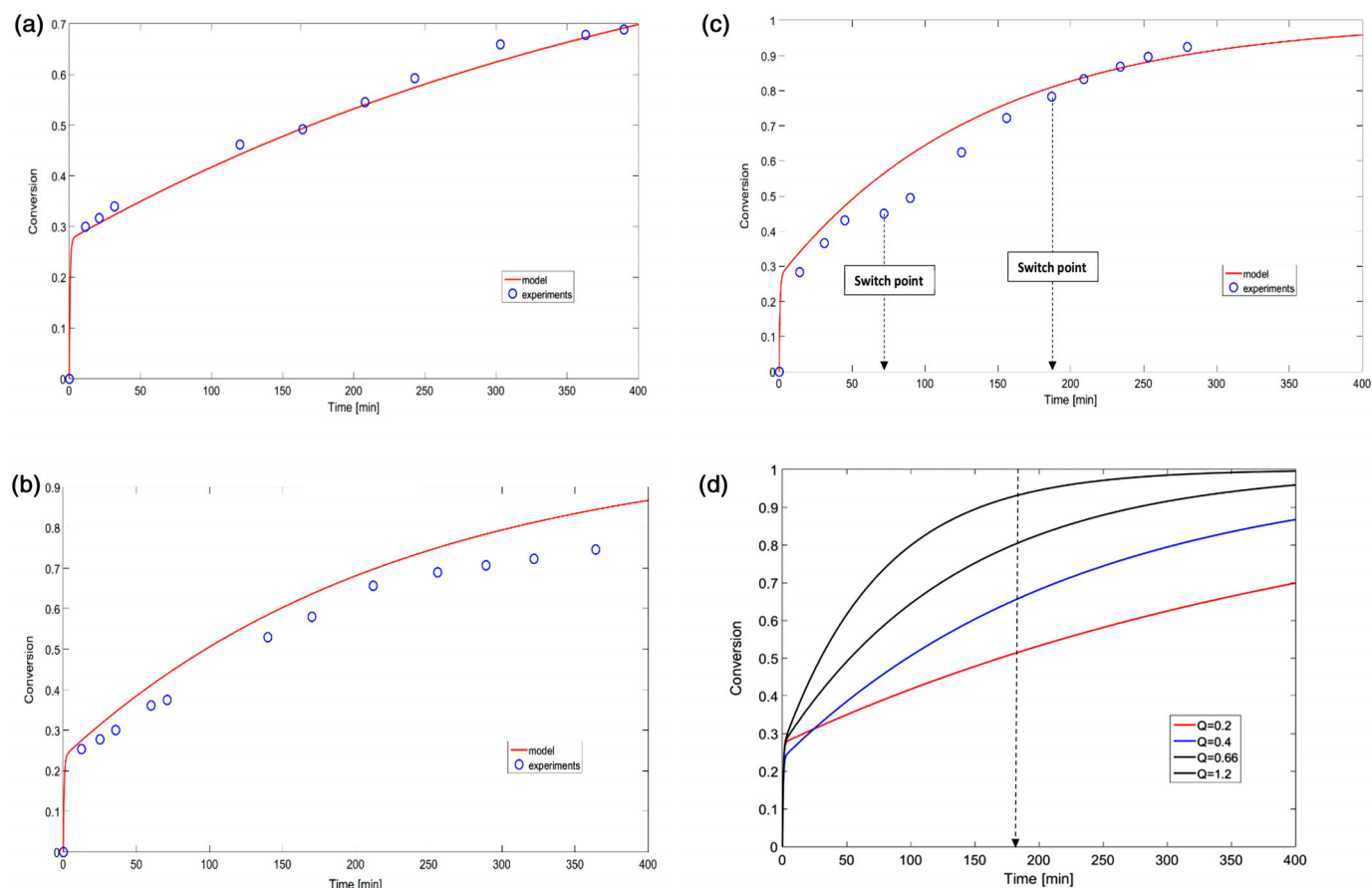


FIGURE 7 Validation of the model of combination of the photoreactor and adsorption column and comparing the results with three process configuration, (a) Case 1, (b) Case 2, (c) Case 3, (d) total flow rate (ml/min) effect on *cis*-cyclooctene conversion [Color figure can be viewed at wileyonlinelibrary.com]

is saturated in less time than the ones used later, so as time increases the packed bed saturation time also increase due to the smaller concentration of *cis*-isomer in the flowing fluid. In Case (c) 90% conversion is achieved after 250 min.

According to the results, Case (c) shows a massive improvement compared to the first two cases. Primarily, using the packed bed with smaller volume gives the chance to quicker recycle the *cis*-isomer. This results in an improvement of the total conversion at any certain time. Also, changing the packed bed as soon as it reaches its saturation point, improves the process performance in terms of an increasing rate of production of the *trans*-isomer. Table 2 summarizes the performance of the different design cases. To give better comparison, we calculate the total conversion divided by the total time of operation for each case which can be correlated to the overall reaction rate of the closed-loop system. As it is expected this number is much higher in Case (c), $0.36 \text{ (min}^{-1}\text{)}$ compared to the Cases (a) and (b), which are 0.175 and $0.2 \text{ (min}^{-1}\text{)}$, respectively.

It is worth mentioning that the outcome of this process configuration has been successfully applied for the photoisomerization of functionalized TCO in our research.⁵⁷

4.5.6 | Flow rate effect

As can be seen in Figure 7d and be expected for a closed-loop recycle flow system, for a certain time of operation, larger flow rates result in a higher conversion. For instance, if the total flow rate is equal to 0.66 ml/min , after almost 3 hr, more than 80% of *cis*-cyclooctene is converted. While, if we double the total flow rate to 1.2 ml/min , a conversion of more than 90% can be reached within 3 hr. On the other hand, if the flow rate is kept lower, for instance 0.2 ml/min , after 3 hr, only 50% of *cis*-cyclooctene is converted. By increasing the total flow rate, although the stable equilibrium may not be reached in photo-microreactor, we get benefit from recycling the feed faster and the whole process speeds up. Therefore, comparing the higher flow rate case with the lower flow rate cases, indicates that in less time of operation, higher conversion is achieved.

5 | CONCLUSION

In this paper, an integrated photo micro-flow adsorption was developed for product separation, with the option to do that in recycle

TABLE 2 Summary of different configuration's performance

	Total flow rate (ml/min)	Time of operation (min)	Total conversion (%)	Conv./time of operation (min ⁻¹)
Case (a)	0.2	400	70	0.175
Case (b)	0.4	365	75	0.2
Case (c)	0.66	250	90	0.36

mode. This was investigated to produce *trans*-cyclooctene from its *cis*-isomer. Here, the thermodynamic equilibrium is shifted by inserting an in-flow separation in a recycling flow mode, which makes better use of the given photoenergy (transport intensification). Further, a full theoretical study of in-flow separation in a recycling flow mode has been conducted. Moreover, different process design options to reach an optimum yield of *trans*-cyclooctene are proposed and experimentally tested. Radiolabeled *trans*-cyclooctenes are valuable in vivo click synthons for PET imaging.

First, the kinetics of the photoisomerization of *cis*- to *trans*-cyclooctene was investigated in a microreactor. Results confirm that the conversion is limited by equilibrium to nearly 28%. The comparison of the reaction rate constants, k_1 and k_{-1} , shows that the reaction rate from *trans*- to *cis*- is higher than *cis*- to *trans*-cyclooctene.

Moreover, an in-depth study of the TCO adsorption on AgNO₃/SiO₂ was done. The results indicate that the adsorption of TCO on AgNO₃ follows the Langmuir isotherm model. The reaction rate is governed by the equilibrium surface reaction. The analysis of the adsorption kinetic data demonstrated that the kinetics can be approximated with a pseudo-second order rate equation. The maximum adsorption capacity of the *trans*-isomer adsorbed per gram AgNO₃ is equal to 44.25 mg_{trans}/g_{silvernitrate}.

The dynamic behavior of the adsorption column was experimentally studied and modeled according to the local equilibrium theory. The results of the model calculations show good agreement with the experimental data. Based on the model, it is possible to predict the breakthrough curve and saturation time of the mentioned adsorption column.

Finally, after optimization of each sub process, that is, photoisomerization and adsorption, three different integrated process designs for photoisomerization of the *cis* to *trans*-isomer was mathematically modeled. According to the calculated model, it is important to remark that by increasing the flow rate a higher conversion of *cis*-isomer was achieved. By increasing the total flow rate, the time that the flow is passing through connecting parts is reduced and also, speeding up the feed recycling gives an advantage. Furthermore, the three different process configurations were tested experimentally. Comparing three cases, Case (c) (Figure 6), shows improvement of the total conversion of the *cis*-isomer. Ninety percent conversion was achieved after 250 min. In Case (c), two parallel photo-microreactors and parallel packed beds in switching mode were applied. Switching the packed bed as soon as it reaches saturation results in obtaining higher conversion in less time. Numbering up the sub processes gives a good promise for scaling up this integrated process.

It is worth mentioning that in this closed-loop system, solvent can be added only once at the beginning. In this system solvent is only carrier medium and is not consumed or converted, thus by recycling, solvent is also recovered and transferred back to the system. As soon as the amount of *cis*-isomer reaches to 0.05 of initial concentration, fixed amount of *cis*-isomer can be added to the initial feed vessel which already contains enough solvent. Therefore, with this closed-loop design, it is possible to reduce the amount of solvent usage to only once.

ACKNOWLEDGMENT

The authors kindly acknowledge the European Research Council for the Advanced Grant on "Novel Process Windows—Boosted Micro Process Technology" No 267443.

AUTHOR CONTRIBUTIONS

Elnaz Shahbazali: Conceptualization; data curation; formal analysis; investigation; methodology; project administration; software; validation; visualization; writing-original draft; writing-review and editing. **Emilie M. F. Billaud:** Conceptualization. **Jan Meuldijk:** Investigation; methodology; supervision; writing-review and editing. **Guy Bormans:** Supervision. **Timothy Noel:** Supervision. **Volker Hessel:** Funding acquisition; supervision; writing-review and editing. **Arash Sarhangi Fard:** Validation; writing-original draft.

ORCID

Elnaz Shahbazali  <https://orcid.org/0000-0003-3817-5263>

REFERENCES

- Fleuren EDG, Versleijen-Jonkers YMH, Heskamp S, et al. Theranostic applications of antibodies in oncology. *Mol Oncol*. 2014;8(4):799-812. <https://doi.org/10.1016/j.molonc.2014.03.010>.
- Lamberts LE, Williams SP, Terwisscha van Scheltinga AG, et al. Antibody positron emission tomography imaging in anticancer drug development. *J Clin Oncol*. 2015;33(13):1491-1504. <https://doi.org/10.1200/JCO.2014.57.8278>.
- Hargreaves RJ. The role of molecular imaging in drug discovery and development. *Clin Pharmacol Ther*. 2008;83(2):349-353. <https://doi.org/10.1038/sj.clpt.6100467>.
- Pien HH, Fischman AJ, Thrall JH, Sorensen AG. Using imaging biomarkers to accelerate drug development and clinical trials. *Drug Discov Today*. 2005;10(4):259-266. [https://doi.org/10.1016/S1359-6446\(04\)03334-3](https://doi.org/10.1016/S1359-6446(04)03334-3).
- Denk C, Svatunek D, Filip T, et al. Development of a ¹⁸F-labeled Tetrizine with favorable pharmacokinetics for bioorthogonal PET imaging. *Angew Chemie Int Ed*. 2014;53(36):9655-9659. <https://doi.org/10.1002/anie.201404277>.

6. Serdons K, Verbruggen A, Bormans GM. Developing new molecular imaging probes for PET. *Methods*. 2009;48(2):104-111. <https://doi.org/10.1016/j.ymeth.2009.03.010>.
7. Blackman ML, Royzen M, Fox JM. Tetrazine ligation: fast bioconjugation based on inverse-electron-demand Diels-Alder reactivity. *J Am Chem Soc*. 2008;130(41):13518-13519. <https://doi.org/10.1021/ja8053805>.
8. Devaraj NK, Upadhyay R, Haun JB, Hilderbrand SA, Weissleder R. Fast and sensitive pretargeted labeling of cancer cells through a tetrazine/trans-cyclooctene cycloaddition. *Angew Chemie - Int Ed*. 2009;48(38):7013-7016. <https://doi.org/10.1002/anie.200903233>.
9. Billaud EMF, Belderbos S, Cleeren F, et al. Pretargeted PET imaging using a bioorthogonal (18)F-labeled trans-Cyclooctene in an ovarian carcinoma model. *Bioconjug Chem*. 2017;28(12):2915-2920. <https://doi.org/10.1021/acs.bioconjchem.7b00635>.
10. Wolf C. Dynamic Stereochemistry of Chiral Compounds.; 2007. doi: <https://doi.org/10.1039/9781847558091>
11. Swenton JS. Photoisomerization of cis-cyclooctene to trans-cyclooctene. *J Org Chem*. 1969;34(10):3217-3218. <https://doi.org/10.1021/jo01262a102>.
12. Royzen M, Yap GPA, Fox JM. A photochemical approach to functionalized trans-cyclooctenes driven by metal complexation. *J Am Chem Soc*. 2008;130:3760-3761.
13. Jimenez-Gonzalez C, Poehlauer P, Broxterman QB, et al. Key green engineering research areas for sustainable manufacturing: a perspective from pharmaceutical and fine chemicals manufacturers. *Org Process Res Dev*. 2011;15(4):900-911. <https://doi.org/10.1021/op100327d>.
14. Poehlauer P, Colberg J, Fisher E, et al. Pharmaceutical roundtable study demonstrates the value of continuous manufacturing in the design of greener processes. *Org Process Res Dev*. 2013;17(12):1472-1478. <https://doi.org/10.1021/op400245s>.
15. Vaccaro L, Lanari D, Marroccoli A, Strappaveccia G. Flow approaches towards sustainability. *Green Chem*. 2014;16(8):3680-3704. <https://doi.org/10.1039/C4GC00410H>.
16. Coyle EE, Oelgemöller M. Micro-photochemistry: photochemistry in microstructured reactors. The new photochemistry of the future? *Photochem Photobiol Sci*. 2008;7(11):1313-1322. <http://xlink.rsc.org/?DOI=b808778d>.
17. Knowles JP, Elliott LD, Booker-Milburn KI. Flow photochemistry: old light through new windows. *Beilstein J Org Chem*. 2012;8:2025-2052. <https://doi.org/10.3762/bjoc.8.229>.
18. Su Y, Straathof NJW, Hessel V, Noël T. Photochemical transformations accelerated in continuous-flow reactors: basic concepts and applications. *Chem - A Eur J*. 2014;20(34):10562-10589. <https://doi.org/10.1002/chem.201400283>.
19. Cambié D, Bottecchia C, Straathof NJW, Hessel V, Noël T. Applications of continuous-flow photochemistry in organic synthesis, material science, and water treatment. *Chem Rev*. 2016;116:10276-10341. <https://doi.org/10.1021/acs.chemrev.5b00707>.
20. Noël T. *Photochemical processes in continuous-flow reactors*. Singapore: World Scientific; 2017.
21. Losey MW, Schmidt MA, Jensen KF. Microfabricated multiphase packed-bed reactors: characterization of mass transfer and reactions. *Ind Eng Chem Res*. 2001;40(12):2555-2562. <https://doi.org/10.1021/ie000523f>.
22. Jensen KF. Microreaction engineering—is small better? *Chem Eng Sci*. 2001;56(2):293-303. [https://doi.org/10.1016/S0009-2509\(00\)00230-X](https://doi.org/10.1016/S0009-2509(00)00230-X).
23. Shang M, Noël T, Su Y, Hessel V. High pressure direct synthesis of Adipic acid from cyclohexene and hydrogen peroxide via capillary microreactors. *Ind Eng Chem Res*. 2016;55(10):2669-2676. <https://doi.org/10.1021/acs.iecr.5b04813>.
24. Carucci JRH, Halonen V, Eränen K, et al. Ethylene oxide formation in a microreactor: from qualitative kinetics to detailed modeling. *Ind Eng Chem Res*. 2010;49:10897-10907. <https://doi.org/10.1021/ie100521j>.
25. Jiang M, Qi Y, Cui YL, Zhao L, Liu S. Removal and recovery of chromium from aqueous solutions by reduction-absorption microreactor. *Water Air Soil Pollut*. 2017;228(1):1-11. <https://doi.org/10.1007/s11270-016-3203-6>.
26. Seeberger PH. Organic synthesis: scavengers in full flow. *Nat Chem*. 2009;1(4):258-260. <https://doi.org/10.1038/nchem.267>.
27. Ley SV, Baxendale IR. New tools and concepts for modern organic synthesis. *Nat Rev Drug Discov*. 2002;1(8):573-586. <https://doi.org/10.1038/nrd871>.
28. Baxendale IR, Ley SV, Mansfield AC, Smith CD. Multistep synthesis using modular flow reactors: Bestmann-ohira reagent for the formation of alkynes and triazoles. *Angew Chemie - Int Ed*. 2009;48(22):4017-4021. <https://doi.org/10.1002/anie.200900970>.
29. Baxendale IR. The integration of flow reactors into synthetic organic chemistry. *J Chem Technol Biotechnol*. 2013;88(4):519-552. <https://doi.org/10.1002/jctb.4012>.
30. Shahbazali E, Spapens M, Kobayashi H, Ookawara S, Noël T, Hessel V. Connected nucleophilic substitution-Claisen rearrangement in flow—analysis for kilo-lab process solutions with orthogonality. *Chem Eng J*. 2015;281:144-154. <https://doi.org/10.1016/j.cej.2015.06.020>.
31. Shahbazali E, Noel T, Volker H. Photo-claisen rearrangement of allyl phenyl ether in micro-flow: influence of phenyl core substituents and vision on orthogonality. *J Flow Chem*. 2016;6(3):252-259. <https://doi.org/10.1556/1846.2016.00029>.
32. Hessel V, Vural Gürsel I, Wang Q, Noël T, Lang J. Potential analysis of smart flow processing and micro process technology for fastening process development: use of chemistry and process design as intensification fields. *Chem Eng Technol*. 2012;35(7):1184-1204. <https://doi.org/10.1002/ceat.201200038>.
33. Hessel V. Novel process windows—gate to maximizing process intensification via flow chemistry. *Chem Eng Technol*. 2009;32(11):1655-1681. <https://doi.org/10.1002/ceat.200900474>.
34. Hessel V, Kralisch D, Kockmann N, Noël T, Wang Q. Novel process windows for enabling, accelerating, and uplifting flow chemistry. *ChemSusChem*. 2013;6(5):746-789.
35. Noël T, Maimone TJ, Buchwald SL. Accelerating palladium-catalyzed C-F bond formation: use of a microflow packed-bed reactor. *Angew Chemie - Int Ed*. 2011;50(38):8900-8903. <https://doi.org/10.1002/anie.201104652>.
36. Naber JR, Buchwald SL. Packed-bed reactors for continuous-flow C-N cross-coupling. *Angew Chemie - Int Ed*. 2010;49(49):9469-9474. <https://doi.org/10.1002/anie.201004425>.
37. Noël T, Kuhn S, Musacchio AJ, Jensen KF, Buchwald SL. Suzuki-miyaura cross-coupling reactions in flow: multistep synthesis enabled by a microfluidic extraction. *Angew Chemie - Int Ed*. 2011;50(26):5943-5946. <https://doi.org/10.1002/anie.201101480>.
38. Tsuneishi H, Tadao Hakushi YI. Singlet- versus triplet-sensitized enantiodifferentiating photoisomerization of cyclooctene: remarkable effects of spin multiplicity upon optical yield. *J Chem Soc, Perkin Trans 2*. 1996;1601-1605. <https://doi.org/10.1017/CBO9781107415324.004>.
39. Wilson MR, Taylor RE. Strained alkenes in natural product synthesis. *Angew Chemie - Int Ed*. 2013;52(15):4078-4087. <https://doi.org/10.1002/anie.201207712>.
40. Molga EJ, Westerterp KR. Principles of chemical reaction engineering. *Ullmann's Encycl Ind Chem*. 2013:5-83.
41. Fogler HS. Elements of chemical reaction engineering. *Chem Eng Sci*. 1999;42:1000. [https://doi.org/10.1016/0009-2509\(87\)80130-6](https://doi.org/10.1016/0009-2509(87)80130-6).
42. Foo KY, Hameed BH. Insights into the modeling of adsorption isotherm systems. *Chem Eng J*. 2010;156(1):2-10. <https://doi.org/10.1016/j.cej.2009.09.013>.
43. Aracil J, Casillas JL, Martinez M. Modelling and solving fixed-bed adsorption. *Mathemat Methods Appl Sci*. 1993;1(1992):533-544.

44. Costa C, Rodrigues A. Design of cyclic fixed-bed adsorption processes. Part I: phenol adsorption on polymeric adsorbents. *AIChE J.* 1985;31(10):1645-1654. <https://doi.org/10.1002/aic.690311008>.
45. Fournel L, Mocho P, Brown R, Le Cloirec P. Modeling breakthrough curves of volatile organic compounds on activated carbon fibers. *Adsorption.* 2010;16(3):147-153. <https://doi.org/10.1007/s10450-010-9207-4>.
46. Siahpoosh M, Fatemi S, Vatani A. Mathematical modeling of single and multi-component adsorption fixed beds to rigorously predict the mass transfer zone and breakthrough curves. *Iran J Chem Chem Eng.* 2009;28(3):25-44.
47. Chuang CL, Chiang PC, Chang EE. Modeling VOCs adsorption onto activated carbon. *Chemosphere.* 2003;53(1):17-27. [https://doi.org/10.1016/S0045-6535\(03\)00357-6](https://doi.org/10.1016/S0045-6535(03)00357-6).
48. Wehner JF, Wilhelm RH. Boundary conditions of flow reactor (reprinted from Chem Engng, vol 6, pg 89-93, 1956). *Chem Eng Sci.* 1995;50(24):3885-3888. [https://doi.org/10.1016/0009-2509\(96\)81815-x](https://doi.org/10.1016/0009-2509(96)81815-x).
49. Lin J, Wang L. Comparison between linear and non-linear forms of pseudo-first-order and pseudo-second-order adsorption kinetic models for the removal of methylene blue by activated carbon. *Front Environ Sci Eng China.* 2009;3(3):320-324. <https://doi.org/10.1007/s11783-009-0030-7>.
50. Simonin JP. On the comparison of pseudo-first order and pseudo-second order rate laws in the modeling of adsorption kinetics. *Chem Eng J.* 2016;300:254-263. <https://doi.org/10.1016/j.cej.2016.04.079>.
51. Ho YS, McKay G. Pseudo-second order model for sorption processes. *Process Biochem.* 1999;34(5):451-465. [https://doi.org/10.1016/S0032-9592\(98\)00112-5](https://doi.org/10.1016/S0032-9592(98)00112-5).
52. Qiu H, Lv L, Pan B, Zhang QQ, Zhang W, Zhang QQ. Critical review in adsorption kinetic models. *J Zhejiang Univ Sci A.* 2009;10(5):716-724. <https://doi.org/10.1631/jzus.A0820524>.
53. Shahwan T. Sorption kinetics: obtaining a pseudo-second order rate equation based on a mass balance approach. *J Environ Chem Eng.* 2014;2(2):1001-1006. <https://doi.org/10.1016/j.jece.2014.03.020>.
54. Song X, Zhang Y, Yan C, Jiang W, Chang C. The Langmuir monolayer adsorption model of organic matter into effective pores in activated carbon. *J Colloid Interface Sci.* 2013;389(1):213-219. <https://doi.org/10.1016/j.jcis.2012.08.060>.
55. Dural MU, Cavas L, Papageorgiou SK, Katsaros FK. Methylene blue adsorption on activated carbon prepared from *Posidonia oceanica* (L.) dead leaves: kinetics and equilibrium studies. *Chem Eng J.* 2011;168(1):77-85. <https://doi.org/10.1016/j.cej.2010.12.038>.
56. Matsui Y, Ando N, Sasaki H, Matsushita T, Ohno K. Branched pore kinetic model analysis of geosmin adsorption on super-powdered activated carbon. *Water Res.* 2009;43(12):3095-3103. <https://doi.org/10.1016/j.watres.2009.04.014>.
57. Billaud EMF, Shahbazali E, Ahamed M, et al. Micro-flow photosynthesis of new dienophiles for inverse-electron-demand Diels-Alder reactions. Potential applications for pretargeted in vivo PET imaging. *Chem Sci.* 2017;8(2):1251-1258. <https://doi.org/10.1039/C6SC02933G>.

SUPPORTING INFORMATION

Additional supporting information may be found online in the Supporting Information section at the end of this article.

How to cite this article: Shahbazali E, Billaud EMF, Fard AS, et al. Photo isomerization of *cis*-cyclooctene to *trans*-cyclooctene: Integration of a micro-flow reactor and separation by specific adsorption. *AIChE J.* 2021;67:e17067. <https://doi.org/10.1002/aic.17067>